**Review article** **Open Access**

Wei Li and Jason G. Valentine*

# Harvesting the loss: surface plasmon-based hot electron photodetection

DOI 10.1515/nanoph-2015-0154
Received December 15, 2015; Revised January 18, 2016; accepted January 25, 2016

**Abstract:** Although the nonradiative decay of surface plasmons was once thought to be only a parasitic process within the plasmonic and metamaterial communities, hot carriers generated from nonradiative plasmon decay offer new opportunities for harnessing absorption loss. Hot carriers can be harnessed for applications ranging from chemical catalysis, photothermal heating, photovoltaics, and photodetection. Here, we present a review on the recent developments concerning photodetection based on hot electrons. The basic principles and recent progress on hot electron photodetectors are summarized. The challenges and potential future directions are also discussed.

**Keywords:** hot electrons; surface plasmons; plasmonics; photodetection; optoelectronics.

## 1 Introduction

Surface plasmons provide a means to enhance light-matter interaction through coherent electron oscillations that lead to strong electromagnetic fields at the surface of metals or any other material with a negative permittivity. In fact, the strong absorption and light scattering inherent in surface plasmon excitation has been used for thousands of years through the incorporation of metal particles in glass to create colorful stained glass windows and goblets [1]. More recently, surface plasmon-based photonics, or "plasmonics" [2–4], has been used for enhancing light-matter interaction at the nanoscale in controlling light propagation [5, 6], emission [7, 8], and concentration [9, 10]. Research on plasmonics has become a flourishing field with numerous applications [11, 12], including metamaterials and metasurfaces [13, 14], sub-diffraction-limited imaging [15], lasers [16], and cloaking [17]. Plasmonics could also be used to enhance the performance of photovoltaic devices [18, 19], photodetectors and modulators [2, 20], and environmental sensors [21, 22].

Surface plasmons exist as either propagating surface plasmon polaritons (SPPs) on planar interfaces or localized surface plasmon resonances (LSPRs) that are confined to the surface of a particle. Surface plasmons are readily damped; thus, after a short time, the plasmon will start to decay radiatively, into reemitted photons [23], or nonradiatively [24–26] via intraband or interband transitions, forming energetic or "hot" electrons. The plasmon decay processes after excitation are illustrated in Figure 1A. The hot electrons will further thermalize through electron-electron and electron-phonon coupling with the energy eventually being transferred to heat. In most cases, the nonradiative plasmon decay will serve as a parasitic process that limits the performance of plasmonic devices [33], for instance, limiting propagation length in plasmonic waveguides. In plasmonic metamaterials, the nonradiative decay process will lead to optical absorption in the metal and reduced performance. Although much effort has been devoted to mitigating plasmon nonradiative decay, recent research has uncovered exciting opportunities for harnessing the process [27, 34], such as in photothermal heat generation [35, 36], photovoltaic devices [27, 37], photocatalysis [38–40], driving material phase transitions [41, 42], photon energy conversion [43], and photodetection [44–50]. For instance, the decay of hot electrons can lead to the local heating of the plasmonic nanostructures, making them candidates for nanoscale heat sources [35, 36] for use in cancer therapy [51] and solar steam generation [52, 53]. On the contrary, hot electrons can be captured before thermalization by an adjacent semiconductor, providing a novel photoelectrical energy conversion scheme for photovoltaics or for driving chemical reactions [39, 40]. In this case, carriers excited with photon energies lower than the semiconductor bandgap can be captured, circumventing bandgap limitations and opening pathways

***Corresponding author: Jason G. Valentine,** Department of Mechanical Engineering, Vanderbilt University, Nashville, TN 37212, USA, e-mail: jason.g.valentine@vanderbilt.edu
**Wei Li:** Department of Mechanical Engineering, Vanderbilt University, Nashville, TN 37212, USA

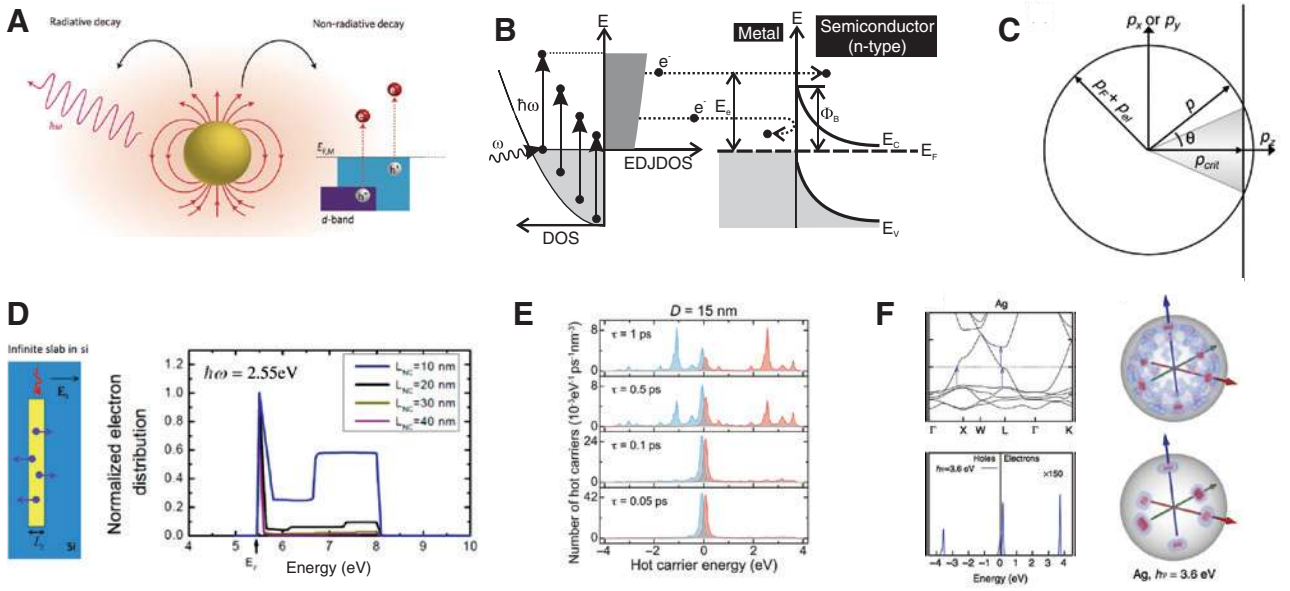


**Figure 1:** (A) Plasmon decay mechanism: The plasmon can either radiatively decay into reemitted photons or nonradiatively decay into hot electrons. (B) Left: Excitation of electrons in the metal from occupied energy levels in the conduction band (shaded gray) to unoccupied levels above the Fermi energy. Right: Energy diagram of the Schottky junction at the metal-semiconductor interface (shown for an n-type semiconductor). Hot electrons with energy larger than the Schottky barrier can be emitted over the barrier into the semiconductor. (C) Schematic showing an isotropic hot electron momentum distribution in a sphere and a limited escape cone. (D) Hot electron distributions in Au slabs as a function of slab thickness. (E) Hot carrier distribution as a function of hot carrier lifetime in silver nanoparticles. Zero energy refers to the Fermi level. (F) Left: Band structures (top) and predicted plasmonic hot carrier energy distributions (bottom) for silver. Right: Anisotropic hot carrier energy (top) and momentum (bottom) distributions in silver. Figures adapted with permission from: (A) Ref. [27], ©2014 Nature Publishing Group; (B) Ref. [28], ©2012 American Institute of Physics; (C) Ref. [29], ©2014 American Institute of Physics; (D) Ref. [30], ©2013 American Chemical Society; (E) Ref. [31] ©2014 American Chemical Society; (F) Ref. [32] ©2014 Nature Publishing Group.

for additional energy harvesting. This review focuses on the recent development of hot electron-based photodetection, and we point the reader to other review articles that cover chemical catalysis and photovoltaic applications [27, 34, 54]. In this article, we will first cover the basic principles underlying hot carrier generation and extraction. Recent developments regarding hot electron-based photodetectors with varying device architectures will then be summarized. Finally, the current challenges and potential future directions will be discussed.

## 2 Hot carrier physics

### 2.1 Internal photoemission

Hot carriers generated in a metal can be collected by placing a semiconductor adjacent to the metal, forming a Schottky barrier. The hot carriers with energy greater than the Schottky barrier can flow into the semiconductor through an internal photoemission process, generating photocurrent (Figure 1B). The very first attempt to quantitatively describe the photon-induced emission of electrons from metals was made by Fowler [55] in the 1930s. Later in the 1950s, the overall hot electron generation and collection process was described by Spicer with an intuitive three-step model [56, 57]: (1) hot electrons are generated in the metal through the absorption of photons, (2) a portion of the hot electrons diffuse to the metal-semiconductor interface before thermalization, and (3) hot electrons with sufficient energy and the correct momentum are injected into the conduction band of the semiconductor through internal photoemission. Therefore, the efficiency of hot carrier devices depends on the initial hot carrier distribution, the transport of the carriers, and the carrier collection efficiency. Fowler's model is perhaps the most widely used description of hot electron injection and is based on a semiclassical model of hot electrons emitted over an energetic barrier, with the critical assumption that the photoexcited electrons in a metal have an isotropic momentum distribution and only the electrons within the momentum cone of the semiconductor can transport across the interface due to the conservation of electron

momentum (Figure 1C). In Fowler's model, the internal photoemission efficiency $\eta$ is given by

$$\eta = \frac{(\hbar\omega - \phi_b)^2}{4E_F\hbar\omega} \quad (1)$$

where $\hbar$ is the reduced Planck constant, $\omega$ is the photon frequency, $E_F$ is the metal Fermi energy, and $\phi_b$ is the barrier height. The barrier height is determined by the work function of the metal and the electron affinity of the semiconductor but can be affected by the fabrication process employed. The experimentally measured Schottky barrier heights for numerous metals and semiconductors are presented in Table 1.

In contrast to the electron-hole pair generation in semiconductors, the efficiency given by Eq. (1) predicts an increasing quantum yield at higher photon energy. Many recently demonstrated hot electron photodetectors based on Schottky barriers have been shown to follow this model [44, 48, 66]. Compared to electron-hole generation and separation in a semiconductor, the internal photoemission over a bulk metal/semiconductor Schottky junction is a very inefficient process. This is mainly due to (1) poor light absorption, (2) a broad hot electron energy distribution [28], and (3) an isotropic hot electron momentum distribution. Surface plasmons can potentially boost the efficiency of hot electron collection by addressing these issues. Plasmonic metallic nanoparticles have an absorption cross-section much larger than the physical size of the particles [67], yielding much more efficient hot electron generation than bulk metal. Plasmonic nanoparticles also produce hot carriers at a higher average energy compared to absorption in bulk metals [30, 31, 68, 69]. Lastly, the momentum distribution of hot carriers can be modified by engineering the modes of the plasmonic structures. Therefore, surface plasmons provide a powerful tool for efficient hot electron generation and extraction [54].

**Table 1:** Experimentally reported Schottky barrier heights $\phi_b$ (eV) for typical plasmonic materials on n-type semiconductors. Data adapted from Refs. [44, 47, 58–65]. For p-type semiconductors, the barrier height can be estimated by subtracting the value from the bandgap energy of the semiconductor.

| | Si | $TiO_2$ | GaAs | Ge | CdSe | CdS |
|---|---|---|---|---|---|---|
| Au | 0.8 | 1.0 | 1.05 | 0.59 | 0.7 | 0.8 |
| Ag | 0.83 | 0.91 | 1.03 | 0.54 | 0.43 | 0.56 |
| Al | 0.81 | Ohmic | 0.93 | 0.48 | N/A | N/A |
| Ti | 0.5 | Ohmic | 0.84 | 0.53 | N/A | 0.84 |
| Cu | 0.8 | 0.85 | 1.08 | 0.5 | 0.33 | 0.5 |
| Pt | 0.9 | 0.73 | 0.98 | 0.65 | 0.37 | 1.1 |
| Cr | 0.6 | 0.88 | 0.82 | 0.59 | N/A | N/A |

## 2.2 Hot carrier generation

Understanding initial hot electron generation and distribution, before inelastic relaxation, is critical to estimating the overall hot carrier injection efficiency. During nonradiative plasmon decay, hot electron-hole pairs are created through Landau damping on a time scale of femtoseconds [70]. Theoretical calculations of hot electron energy distribution in bulk metal, based on the electron density of states approximated by a free electron gas model, shows a broad continuous distribution of hot electron energies upon excitation [28] (Figure 1B). This broad hot electron energy distribution sets an impediment for realizing high efficiency in the internal photoemission process, as many carriers will have an energy that is below the Schottky barrier [28]. In contrast to bulk metals, it has been shown that the hot carrier energy distribution in plasmonic nanoparticles can potentially be narrowband [30, 31, 69, 71, 72] and is strongly dependent on the particle size [30, 69] and geometry [71, 73, 74] (Figure 1D). For instance, hot carriers are more efficiently generated in small plasmonic nanoparticles compared to large ones [30]. Nanoparticle geometry, including shape [71] and aspect ratio [75], also plays an important role in determining the hot carrier generation and injection due to carrier confinement and surface scattering [71]. In addition, a theoretical model for the hot carrier generation process has been developed using Fermi's golden rule, where the conduction electrons are described as free particles in a confined potential well [31]. This model predicts that both the production rate and the energy distribution of the hot carriers are strongly dependent on the particle size and hot carrier lifetime. In addition to energy distribution, the hot carrier momentum distribution is also an important factor. Hot carriers are primarily generated with momentum parallel to the external field [31], which is generally parallel with the semiconductor interface in the case of an antenna, resulting in poor injection. Moreover, hot electron generation is also dependent on the plasmonic material employed [32, 72, 76–78]. Several groups have explored the effects of the electronic structure of the metal on the generated carrier distributions [32, 76] (Figure 1F), and it has been shown that, in the interband transition regime, the electronic band structure of the metal plays an important role in determining both the energy and the momentum distribution of the generated hot carriers [32]. In fact, in this regime, none of the commonly used plasmonic materials, including gold, silver, aluminum, and copper, exhibit the isotropic momentum distribution assumed in Fowler's theory [32]. Additionally, the effects of phonons and surfaces on hot carriers have also been studied [79].

Therefore, one needs to take plasmonic nanostructure geometry, size, excitation condition, hot carrier lifetime, and material electronic band structure into account when optimizing hot carrier device efficiency.

# 3 Photodetection with hot electrons

## 3.1 Free-space photodetectors

Early work on free-space photodetectors based on internal photoemission dates back almost half a century. In 1967, Peters demonstrated a photodetector using internal photoemission to detect low-energy, infrared photons [80]. Later, free-space photodetectors based on this principle were developed for both Schottky [81, 82] and MIM [83, 84] diodes. Over the past few years, this area has seen renewed interest due to the advances in plasmonics, which provide a mechanism for strong light-matter interaction and enhanced resonant absorption and photoemission. One of the key features of hot electron injection is that it enables sub-bandgap photodetection. Therefore, hot electron photodetectors based on silicon [44–46, 48, 49, 85–91] can be potentially employed in the telecommunications band, avoiding the need to use InGaAs and Ge detectors. In addition, the tunability of the plasmonic structures enables a straightforward means to tailor the response of a photodetector including the working wavelength, bandwidth, and polarization dependence [44, 46, 48, 49]. For more information on general sub-bandgap photodetection we point the reader to a recent review on the topic [92].

In 2011, Knight et al. demonstrated a free-space hot electron photodetector based on a plasmonic nanoantenna

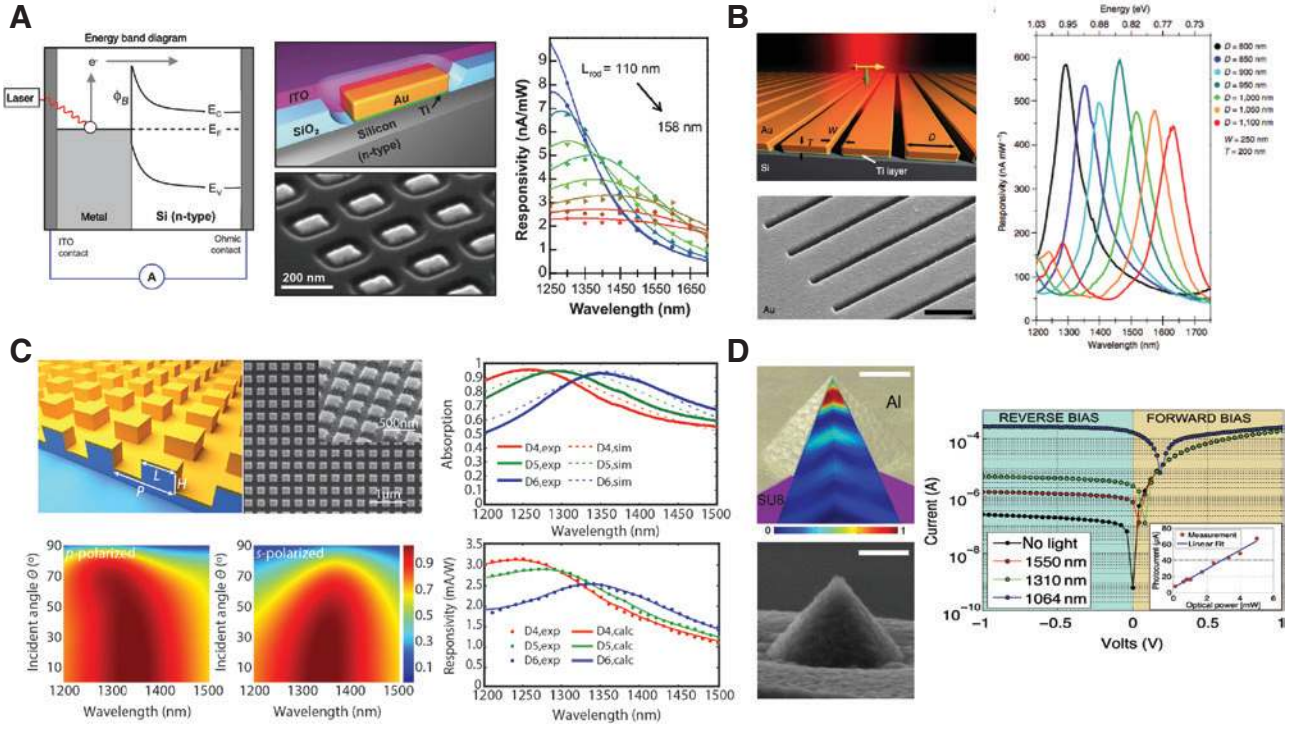


**Figure 2:** Schottky interface-based free-space hot electron photodetectors.
(A) Left: Band diagram for plasmonically driven internal photoemission over a nanoantenna-semiconductor Schottky barrier. Middle: Schematic and scanning electron micrograph (SEM) of a representative device. Right: Experimental photocurrent responsivity for nine different antenna lengths. (B) Left: Schematic (top) and SEM (bottom) of a gold grating on an n-type silicon substrate with 2 nm Ti adhesion layer. Right: Narrowband photoresponsivity spectrum. (C) Left: Schematic and SEM of the metamaterial perfect absorber-based hot electron photodetector (top). Omnidirectional absorption for s- and p-polarization (bottom). Right: Experimentally measured optical absorption and photoresponsivity spectrum. (D) Left: Theoretical normalized average electromagnetic field intensity distribution (top) and SEM (bottom) of a silicon pyramid hot electron detector. Right: I-V measurements of the device at constant power for three different wavelengths. The inset shows the power dependent photocurrent. Figures adapted with permission from: (A) Ref. [44], ©2011 American Association for the Advancement of Science; (B) Ref. [46], ©2013 Nature Publishing Group; (C) Ref. [48], ©2014 American Chemical Society; (D) Ref. [90], ©2015 Optical Society of America.

and silicon, with the ability to detect near-infrared light below the silicon bandgap energy [44] (Figure 2A). In this device, the plasmonic nanoantenna serves simultaneously as the free-space light collector and electron emitter. After the nonradiative decay of surface plasmons, hot electrons are generated and injected into the conduction band of the n-type silicon substrate followed by the collection through an ohmic contact on the silicon. The top contact is formed by putting an indium tin oxide (ITO) conduction layer on top of the plasmonic antenna. By tuning the geometry of the plasmonic nanoantenna, one can control the absorption spectrum and therefore the photoresponsivity spectrum. Plasmonic gratings can also be used to realize selective, narrowband hot electron photodetectors [46] (Figure 2B). The extraordinary optical transmission observed in periodic gratings can strongly couple the free-space light into SPPs, resulting in a strong, narrowband resonant absorption. The electrically connected metallic grating structures also facilitate electron transport. Such gratings have been shown to possess a photoresponsivity of 0.6 mA/W and an internal quantum efficiency of 0.2%, a roughly 20 times improvement over the nanoantenna devices. A hot electron photodetector with further enhanced efficiency was demonstrated [48] (Figure 2C) by integrating the concept of metamaterial perfect absorbers [93, 94] with the hot electron transfer process. The perfect absorption of light is realized by overlapping the LSPR with a Fabry-Perot resonance in the silicon cavity. Interestingly, this perfect absorption can be realized within a gold film of only 15 nm. This feature brings two advantages: (1) hot electrons are efficiently generated via the perfect absorption and (2) all the hot electrons are generated close to the Schottky interface, ensuring an efficient transport to the interface. This perfect absorber hot electron detector has been shown to exhibit a photoresponsivity of more than 3 mA/W while also preserving an omnidirectional response at a wavelength of about 1300 nm [48]. The bandwidth can also be broadened by integrating multiple resonators [48]. Pyramid nanostructures [90] have also been shown to enhance the photoresponsivity of hot electron detectors (Figure 2D). In this device, the silicon pyramids perform as efficient and broadband light concentrators, focusing the light from a large area into a small active pixel area where the hot electrons are generated. Metal layers are deposited on top of the silicon pyramids so that the Schottky interface is only formed at the apex region of the pyramids, ensuring a small dark current. More importantly, nanoscale confinement of plasmons at the apex of the tip plays a role in efficiency enhancement by relaxing momentum mismatch [71, 95]. Operating at 0.1 V reverse bias, a responsivity of 5 and 12 mA/W at 1550 and 1300 nm, respectively, has been demonstrated. In addition, large area and low-cost fabrication techniques [88, 89] can be used for silicon-based hot electron photodetectors. Hot electron photodetectors can be employed in the visible regime [58, 96–99] by swapping silicon with larger bandgap materials such as $TiO_2$ [58, 96–98, 100, 101] and ZnO [99]. These detectors have much higher efficiencies than their telecommunication band counterparts due to the higher photon energy of visible light. Tandem-structured devices with double Schottky barriers can also be used to further enhance hot electron collection efficiency [102].

An alternative approach to extracting hot electrons is to form a metal-insulator-metal diode [47, 83, 84, 103–107]. MIM diodes have been used as “rectennas” [108] at infrared and lower frequencies for power conversion and transmission. At optical frequencies, the operation of MIM diodes as rectification antennas has proven to be difficult [109], with efficiencies remaining low [110] due to the limitation on the RC time constant of the MIM diodes. However, the generation of hot electrons circumvents this limitation: hot electrons generated in one metal can tunnel through the thin insulating layer and be collected in the other metal contact, leading to a measurable photocurrent. Similar to the three-step model [56, 57], the photoemission of carriers across a MIM diode can be described in a series of five steps [103] as depicted in the band diagram shown in Figure 3A. This is similar to the junctions in plasmonic nanogap antennas [110, 113], where electrons can tunnel through the nanogap leading to photocurrent (Figure 3B). In the MIM diode, the hot electrons can be generated in both metal contacts; therefore, the key here is to create asymmetric hot electron generation or transport in the top and bottom metal layers. This can be done by creating asymmetric absorption, creating asymmetric barrier heights using different metals, or applying a bias to the device. In 2011, a hot electron-based MIM device [104] was proposed using an Au-$Al_2O_3$-Au diode for the application of solar energy conversion and photodetection (Figure 3C). In this planar unpatterned diode, a Kretschmann prism coupling configuration was used to couple the incident light to one of the electrodes, creating asymmetric absorption. This work predicted an optimized efficiency of 2.7% under AM 1.5 G illumination. The asymmetric hot electron generation in the top and bottom contacts can also be realized by creating LSPRs in one of the contacts [103, 105, 114, 115]. It has been shown that asymmetric hot electron generation and enhancement of hot electron emission in Au-$Al_2O_3$-Au MIM diodes can be realized by reshaping the top metallic film contact into stripes [103] (Figure 3D). The stripes support

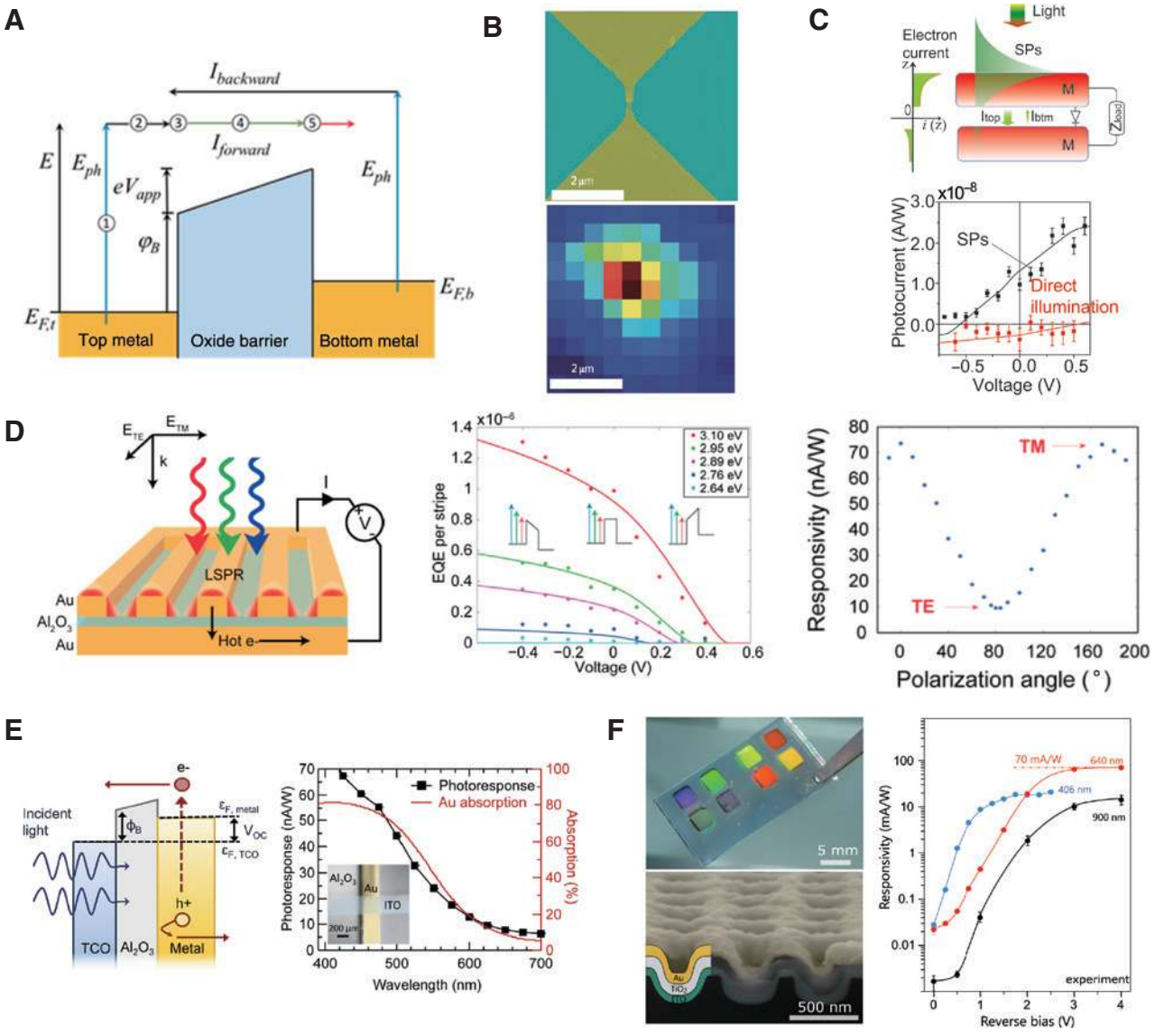


**Figure 3:** Free-space hot electron photodetectors based on MIM and metal-insulator-TCO junctions.
(A) Band diagram for a metal-insulator-metal diode. Hot electrons can be generated in either contact and get collected through five consecutive steps. (B) Colorized SEM image (top) and photocurrent map (bottom) of a plasmonic nanogap antenna. Electrons can tunnel through the nanogap and generate photocurrent. (C) Top: Schematic of the MIM device. With a hot electron density difference in the top and bottom electrodes, forward current $I_{top}$ overwhelms back current $I_{btm}$. Surface plasmons excited on one electrode can largely increase output current. Bottom: Measured photocurrent with surface plasmon excitation. (D) Left: Schematic illustration of a MIM junction formed between a wide bottom electrode and a set of nanoscale top electrodes, working under TM illumination. Middle: Dependence of the device external quantum efficiency on applied voltage and incident photon energy. Right: Dependence of the device photoresponsivity on incident light polarization, indicating the role of surface plasmons. (E) Left: Band diagram of a metal-insulator-TCO junction. Light is illuminated from the TCO side. Hot electrons are only generated in the metal side. Right: Photoresponse and Au absorption spectrum in the visible regime, indicating that the photocurrent comes from hot electrons generated in the gold electrode. (F) Left: Photograph and SEM image of a Au-$TiO_2$-ITO plasmonic crystal detector. Right: Responsivity as a function of applied reverse bias at three different illumination wavelengths. Figures adapted with permission from: (A) Ref. [103], ©2014 American Chemical Society; (B) Ref. [110], ©2010 Nature Publishing Group; (C) Ref. [104], ©2011 American Chemical Society; (D) Ref. [103], ©2014 American Chemical Society; (E) Ref. [111] ©2015 American Chemical Society; (F) Ref. [112] ©2015 American Chemical Society.

an LSPR under TM illumination; therefore, the incoming light is mostly absorbed in the top contact. As a result, a measurable photocurrent is observed in the diode even without external bias. The stripe width-dependent and polarization-dependent photocurrent observed in this study further indicates that one needs to take the spatial

and vectorial properties of the hot electron generation along with the material selection and diode geometry into account when designing the device.

Recently, researchers have explored new schemes to extract hot electrons for photodetection using transparent conducting oxides (TCO), including metal-insulator-TCO [111] and metal-semiconductor-TCO [112, 116] junctions (Figure 3E and F). The use of TCO allows efficient electron collection while leading to asymmetric absorption and hot carrier generation yielding an efficient net photocurrent. In both schemes, light can be incident from the TCO side. Because the absorption of TCO is small, most of the incident light is absorbed in the metal layer and in the vicinity of the metal-insulator/semiconductor interface, leading to highly asymmetric and efficient hot carrier generation [111]. Therefore, opposed to planar MIM diodes [104], special coupling is not necessary. The TCO-based structures have been demonstrated to produce responsivity up to 70 mA/W under a reverse bias of –3 V in the visible regime [112] (Figure 3F). In terms of detection speed, recent ultrafast studies on hot electron relaxation dynamics [117] have revealed hot electron relaxation times as fast as ~45 fs. Furthermore, the speed was strongly dependent on the local field enhancement and therefore can be controlled by tailoring the plasmonic geometry. These results indicate that the ultimate detection speed of hot electron devices could be extremely fast, although more work is still needed to understand the response time of a full device.

## 3.2 On-chip photodetectors

Hot electrons have also played a role in realizing on-chip photodetectors based on silicon with several demonstrations [45, 85, 87, 118–123] over the past several years. Despite the success of using silicon photonics for controlling light emission, propagation, and modulation, the use of silicon as an active absorbing material in the telecommunication band is challenging due its transparency in this regime. Efforts focused on developing complementary metal-oxide semiconductor (CMOS)-compatible, silicon-based on-chip photodetectors include using cavity-enhanced absorption [124], two-photon absorption (TPA) [125], and mid-bandgap generation [126]. These approaches usually involve complicated fabrication processes or limit the operational bandwidth and power range. The use of hot electrons for photodetection can be employed by simply placing metal contacts on top of the silicon waveguide. The metal-silicon interface simultaneously serves as a Schottky interface for electrons and a metal-dielectric interface supporting SPP modes. A waveguide-based geometry can enable a higher internal quantum efficiency than free-space plasmonic antenna-based geometries due to two reasons. First, the SPPs propagate along the metal dielectric interface, naturally generating hot electrons in the vicinity of the Schottky interface. Second, in contrast to plasmonic antennas in which the electric field is primarily parallel to the Schottky interface, the SPPs have an electric field component perpendicular to the interface, therefore preferentially generating hot electrons with a momentum vector perpendicular to the Schottky interface.

Researchers have proposed [118, 119] and experimentally demonstrated [120] waveguide-based Schottky detectors by putting metal stripes on silicon, forming SPP waveguides (Figure 4A). Internal responsivity of 0.38 and 1.04 mA/W were measured at a wavelength of 1280 nm [120] for gold and aluminum stripes on n-type silicon, respectively. A silicon waveguide-based SPP Schottky photodetector operating at telecom wavelengths has also been developed [45] (Figure 4B). The device was fabricated using a self-aligned approach of local oxidation of silicon (LOCOS) on a silicon on insulator substrate (Figure 4B). Internal responsivity of 0.25 and 13.3 mA/W were measured for wavelengths of 1.55 and 1.31 μm under a reverse bias of 0.1 V [45]. Later, an internal responsivity of 12.5 mA/W at a wavelength of 1.55 μm [85] was demonstrated by optimizing the device design (Figure 4C). Other than improving the photoresponsivity, there are also efforts focused on improving the detection speed of on-chip hot electron photodetectors [88, 121, 122] by minimizing the junction capacitances of the photodetector. This is realized by reducing the metal-semiconductor contact area by directly depositing the metal contact on the vertical output facet of the waveguide (Figure 4D). With this detection scheme, a bandwidth up to 1 GHz has been achieved while also maintaining a responsivity of 3.5 mA/W at a negative bias of –21 V [122]. Recently, the bandwidth is further improved and a hot electron photodetector with data reception rate of 40 Gbit/s has been demonstrated [128]. A Schottky detector has also been applied to Si-cored fiber [129] for applications such as power monitoring in optical fiber communication. Other than using Schottky interfaces on silicon waveguides, MIM diodes have also been used in a waveguide geometry [127] (Figure 4E). MIM diodes can be built on a wider range of devices such as polymer waveguides and optical fiber. In addition, multiple metal contacts [87, 120–122] are not required here, simplifying the geometry [47, 104], although quantum efficiency suffers when compared to a Schottky diode.

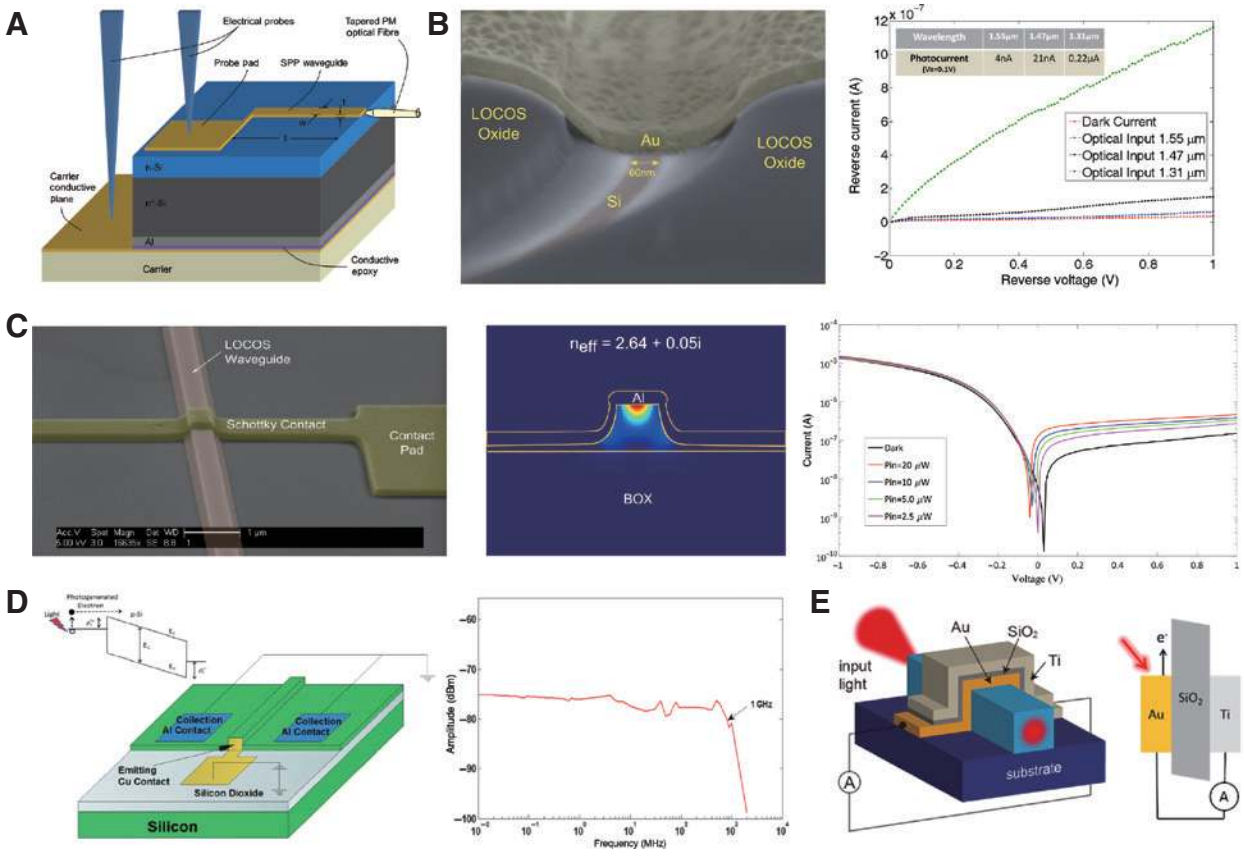


**Figure 4:** On-chip hot electron photodetectors.
(A) Schematic of the SPP photodetector. Light is coupled to a SPP waveguide with optical fiber. One metal contact is connected to the SPP waveguide and the other is connected to the bottom of the semiconductor. (B) Left: SEM image of the locally oxidized silicon bus waveguide integrated with the Schottky photodetector. Right: Photocurrent as a function of reverse voltage for three different wavelengths. (C) Left: SEM image of the photonic bus waveguide integrated with the Schottky photodetector. Middle: Intensity mode profile of the waveguide. Right: Photocurrent as a function of reverse voltage and illumination power. (D) Left: Schematic of the Cu/Si photodiode, with metal contact on the vertical output facet of the waveguide. Right: Experimental frequency response of the detector showing up to 1 GHz operational frequency. (E) Schematic (left) and energy (right) diagram of a MIM diode detector integrated with optical waveguide. Figures adapted with permission from: (A) Ref. [120], ©2010 Optical Society of America; (B) Ref. [45], 2011 ©American Chemical Society; (C) Ref. [85], ©2012 Optical Society of America; (D) Ref. [122], ©2013 American Institute of Physics; (E) Ref. [127] ©2014 American Chemical Society.

## 3.3 Hot electrons with 2D materials

Over the past decade, the unique properties of graphene and other 2D materials, such as transition metal dichalcogenides, have made them attractive for optoelectronic and photonic applications [130–132]. The high electron mobility, broadband absorption, ultrafast response, and electrical tunability of these 2D material systems enables their application in ultrafast and ultrasensitive light detection [133, 134]. However, due to their atomic thickness, the light-matter interaction in 2D materials is usually limited. On the contrary, plasmonics enable strong light-matter interaction with 2D materials due to high field concentration [135–138]. Additionally, it has been shown that surface plasmons in metallic nanoparticles can directly interact with 2D materials through hot electron injection [42, 139–143]. For instance, hot electrons can change the doping of graphene [140] or molybdenum disulfide ($MoS_2$) [42, 143], leading to structural phase transitions [42] or modulation of the absorption spectrum [143]. Hot electrons can also be used for enhancing $MoS_2$ photocatalysis of hydrogen evolution [144] and the photoluminescence of $MoS_2$ [141]. A photodetector based on hot electron injection into graphene has also been reported [139] (Figure 5A). In this device, nanoscale plasmonic antennas are sandwiched between two graphene monolayers. Surface plasmons enhance the photocurrent in two ways: by transferring hot electrons generated from plasmon decay in the antenna and by enhancing the near-field and direct electron-hole pair generation in graphene [139, 146]. The contribution of

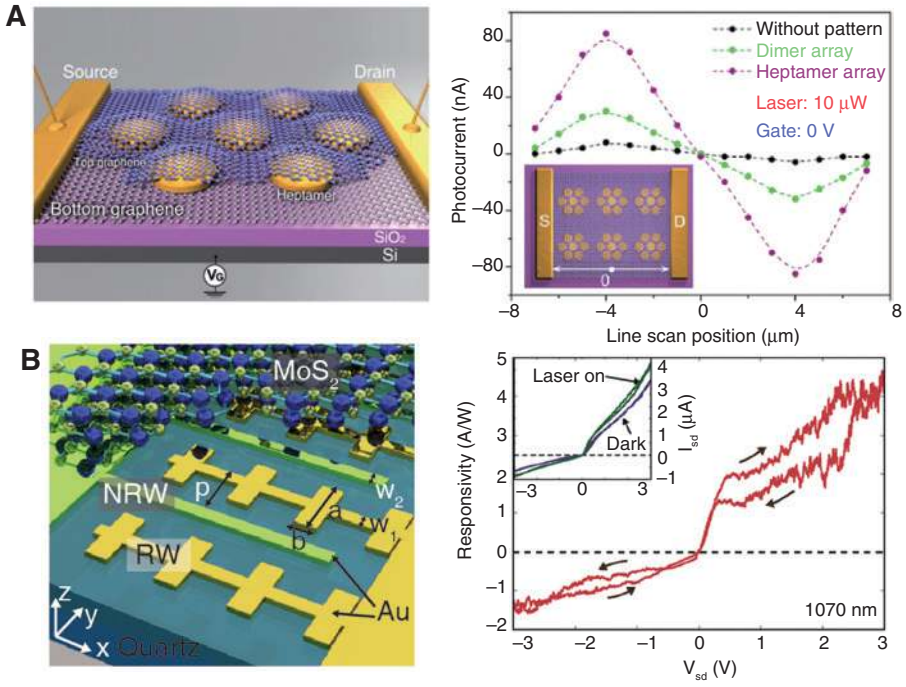


**Figure 5:** Hot electron photodetection based on 2D materials.
(A) Left: Schematic of a graphene-antenna sandwich photodetector. Right: Photocurrent characterization of the graphene-antenna sandwich photodetector showing that the heptamer array is more efficient than a dimer array. (B) Left: Schematic of the Au-$MoS_2$ device in which the yellow Au structures are resonant, whereas the green Au structures are nonresonant. Right: Photoresponsivity as a function of source-drain voltage ($V_{sd}$) measured at 1070 nm. The inset shows the source-drain current ($I_{sd}$) as a function of $V_{sd}$ under illumination and in a dark environment. Figures adapted with permission from: (A) Ref. [139], ©2012 American Chemical Society; (B) Ref. [145], ©2015 American Chemical Society.

direct photoexcitation and hot carrier injection was also investigated by femtosecond pump-probe measurements [146]. In addition, $MoS_2$ has also been used for extracting hot electrons generated from plasmonic nanostrucutres [42, 144, 145]. Photodetectors working in the near-infrared regime with photoresponsivity on the level of A/W have been demonstrated (Figure 5B) by combining photogain in bilayer $MoS_2$ with hot electron injection, although the large responsivity is accompanied by a relatively slow response time [145]. Further research in this direction is needed as novel functionalities and unprecedented performance could potentially be realized by combining hot electron injection with new 2D materials such as InSe [147] and $WS_2$ [148].

## 3.4 Novel functionalities

Research in the emerging field of hot electron photodetection has not only focused on improving the efficiency but also on exploring novel functionalities, which do not exist in conventional semiconductor photodetectors. For instance, nanoscale surface imaging can be realized using the hot electron injection from a plasmonic nanotaper (Figure 6A). A gold nanotaper adiabatically compresses the SPPs at the end of the tip before injecting the electrons into the semiconductor substrate. By scanning the plasmonic nanotaper on the semiconductor, the local chemical sensitivity of the semiconductor surface can be obtained from the hot electron photocurrent map (Figure 6A). In addition, one can use the tunability of plasmonic structures to tailor the response of the photodetector including the working wavelength, bandwidth, and polarization dependence [44, 46, 48, 49, 103, 149]. Recently, a circularly polarized light detector was demonstrated by combining a chiral metamaterial with hot electron injection [49] (Figure 6B). The chiral metamaterial can perfectly absorb circularly polarized light with one particular handedness while largely reflecting the complimentary component. Therefore, it can selectively generate hot electrons and produce a photocurrent signal depending on the handedness of light [49]. This ultracompact detector avoids the complexity of conventional circularly polarized light detection schemes, where a quarter wave-plate and polarizer are used. Another example of a hot electron photodetector with tailored responsivity is a narrowband photodetector

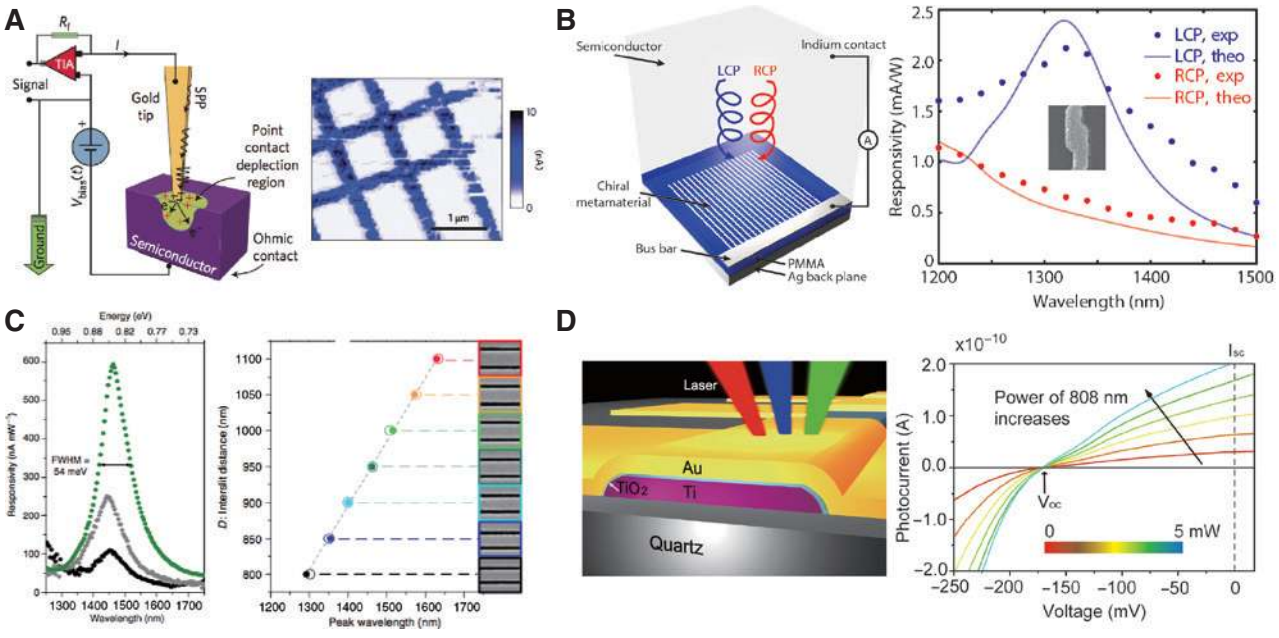


**Figure 6:** Hot electron-enabled novel detection functionalities.
(A) Left: Schematic of hot electron nanoscopy. The gold taper adiabatically compresses the SPPs, providing hot electrons with momentum perpendicular to the semiconductor surface. Right: Hot electron map generated by the nanotaper. (B) Left: Schematic of a circularly polarized light detector combining a silver chiral metamaterial and silicon. Right: Experimentally measured responsivity spectrum for left and right hand circularly polarized light. (C) Left: Narrowband responsivity spectrum of a plasmonic grating-based hot electron detector. Right: The responsivity peak position shows a linear dependence on the interslit distance. (D) Left: Schematic of a MIM diode for wavelength determination. Right: Photocurrent under bias and 808 nm illumination at different powers showing constant open-circuit voltages. Figures adapted with permission from: (A) Ref. [95], ©2013 Nature Publishing Group; (B) Ref. [49], ©2015 Nature Publishing Group; (C) Ref. [46], ©2013 Nature Publishing Group; (D) Ref. [47], ©2013 Nature Publishing Group.

[46] (Figure 6C). The narrowband responsivity comes from the narrowband absorption of the plasmonic grating that supports extraordinary optical transmission. One can also easily tune the responsivity peak position by changing the interslit distance. This narrowband photodetector could find applications in biomedical sensing, imaging, and surveillance where a small wavelength bandwidth is needed, whereas other bands must be suppressed. Another way to perform wavelength-sensitive detection is using the MIM diode (Figure 6D). It has been demonstrated that MIM diodes can be used for direct wavelength determination and real-time deconvolution of multiples signals at different wavelengths based on electron tunneling [47]. In this case, the open-circuit voltage between the upper and lower electrodes in the MIM diode is directly related to the incident photon energy and is not dependent on incident power. This detector provides simplicity compared to grating-based spectroscopy and could potentially lead to the realization of on-chip spectrometry. With the compactness, tunability, and novel functionalities of hot electron detectors, we believe that hot electron photodetectors enabling the full characterization of light (polarization, wavelength, and wave vector) could be realized in a highly integrated platform.

## 4 Future developments and perspectives

Research on plasmon-induced hot electron injection has experienced much progress over the past several years. However, an improvement in device performance is needed to address practical applications. Progress will require improving the efficiency of hot carrier generation and the subsequent transport and injection processes. This involves both the judicious design of plasmonic nanostructures and a better fundamental understanding of the hot carrier generation, transport, and extraction processes.

In terms of plasmonic design, ways to further enhance the field concentration and absorption in ultrathin or small nanoparticles is needed [44, 48, 90, 150]. In terms of hot carrier transport, employing higher-quality noble metals [151, 152] or exploring new plasmonic materials [72,

153–156] could potentially result in longer hot carrier diffusion lengths. Hot electrons can also experience significant reflection as a result of the large wave-vector contrast at the metal-dielectric interface. As such, more work is needed in the design of plasmonic nanostructures that support the generation of hot electrons with a momentum distribution that matches well with the band structure of the semiconductor. For instance, the recent investigation that uses plasmonic tips to adiabatically compress the SPPs, producing hot electrons with momentum perpendicular to the interface, demonstrated a greatly enhanced efficiency [95]. Hot electron transfer efficiencies can further be boosted by embedding the plasmonic nanostructures within the semiconductor, providing more momentum space for hot electron emission [86] (Figure 7A). In addition, it has been shown that the preferred carrier type for extraction, either electrons or holes, is dependent on the plasmonic material employed [32, 72].

A more fundamental understanding of hot carrier generation, transport, and emission is still needed for designing efficient hot carrier devices. For hot carrier distribution, although much work has been devoted to providing theoretical predictions of hot carrier distribution in plasmonic nanostructures [30, 31, 69, 71, 72, 158], more experimental work is needed to validate these models. In addition, a better understanding of the hot carrier relaxation timescale [75, 117, 159–161] in various materials as well as the transport dynamics in nanostructures would provide more valuable information for designing plasmonic devices with efficient hot carrier transport to the Schottky interface. Lastly, engineering the metal-semiconductor interface on the atomic level could also lead to improved hot electron transfer efficiencies [157, 162]. For instance, a recent report describing hot electron transfer by a plasmon-induced interfacial charge-transfer transition has shown an internal quantum efficiency up to 20% independent of incident photon energy [157].

In conclusion, we have reviewed the recent developments in the field of hot electron-based photodetection ranging from fundamental studies regarding hot carrier generation and extraction to hot electron devices for both free-space and on-chip photodetection. Although we have focused on the hot electron-based photodetection, the basic principles and designs presented here can be applied to any system where charge separation is involved, such as photovoltaics [27, 34, 102], photocatalysis [27, 39, 40], as well as light emission [43] and modulation [143]. There are many open challenges in the field such as establishing a better understanding of the carrier injection process, characterizing device speed, and exploring a wider range of plasmonic materials. Ultimately, we believe that advances in these areas should lead to a wealth of opportunities and scientific breakthroughs in the future.

**Acknowledgments:** W.L. and J.G.V. were supported by the National Science Foundation (NSF) under the program CBET-1336455.

**Competing financial interests:** The authors declare no competing financial interests.

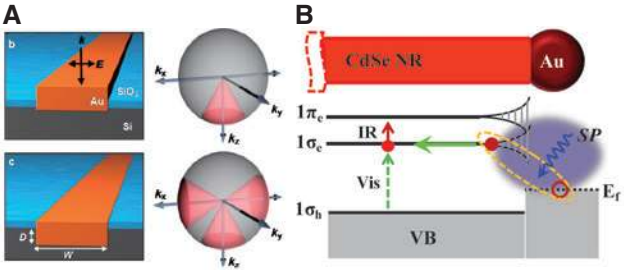


**Figure 7:** Improving the hot electron transfer efficiency.
(A) Embedding plasmonic nanostructures provides more electron escape cones than planar devices. (B) Electronic band structure of a CdSe-Au interface showing the plasmon-induced interfacial charge-transfer transition. The plasmon decay directly creates an electron in the conduction band of the semiconductor and a hole in the metal. Figures adapted with permission from: (A) Ref. [86], ©2013 American Chemical Society; (B) Ref. [157], ©2015 American Association for the Advancement of Science.

## References

[1] Freestone I, Meeks N, Sax M, Higgitt C. The lycurgus cup–a Roman nanotechnology. Gold Bull 2007;40:270–7.
[2] Schuller JA, Barnard ES, Cai W, Jun YC, White JS, Brongersma ML. Plasmonics for extreme light concentration and manipulation. Nat Mater 2010;9:193–204.
[3] Gramotnev DK, Bozhevolnyi SI. Plasmonics beyond the diffraction limit. Nat Photonics 2010;4:83–91.
[4] Stockman MI. Nanoplasmonics: past, present, and glimpse into future. Opt Express 2011;19:22029–106.
[5] Soukoulis CM, Wegener M. Past achievements and future challenges in the development of three-dimensional photonic metamaterials. Nat Photonics 2011;5:523–30.
[6] Yu N, Capasso F. Flat optics with designer metasurfaces. Nat Mater 2014;13:139–50.
[7] Curto AG, Volpe G, Taminiau TH, Kreuzer MP, Quidant R, van Hulst NF. Unidirectional emission of a quantum dot coupled to a nanoantenna. Science 2010;329:930–3.
[8] Ayala-Orozco C, Liu JG, Knight MW, et al. Fluorescence enhancement of molecules inside a gold nanomatryoshka. Nano Lett 2014;14:2926–33.
[9] Kim S, Jin J, Kim YJ, Park IY, Kim Y, Kim SW. High-harmonic generation by resonant plasmon field enhancement. Nature 2008;453:757–60.

[10] Berthelot J, Aćimović SS, Juan ML, Kreuzer MP, Renger J, Quidant R. Three-dimensional manipulation with scanning near-field optical nanotweezers. Nat Nanotechnol 2014;9:295–9.
[11] Dionne JA, Baldi A, Baum B, et al. Localized fields, global impact: industrial applications of resonant plasmonic materials. MRS Bull 2015;40:1138–45.
[12] Fang Z, Zhu X. Plasmonics in nanostructures. Adv Mater 2013;25:3840–56.
[13] Valentine J, Zhang S, Zentgraf T, et al. Three-dimensional optical metamaterial with a negative refractive index. Nature 2008;455:376–9.
[14] Yu N, Genevet P, Kats MA, et al. Light propagation with phase discontinuities: generalized laws of reflection and refraction. Science 2011;334:333–7.
[15] Fang N, Lee H, Sun C, Zhang X. Sub-diffraction-limited optical imaging with a silver superlens. Science 2005;308:534–7.
[16] Oulton RF, Sorger VJ, Zentgraf T, et al. Plasmon lasers at deep subwavelength scale. Nature 2009;461:629–32.
[17] Cai W, Chettiar UK, Kildishev AV, Shalaev VM. Optical cloaking with metamaterials. Nat Photonics 2007;1:224–7.
[18] Atwater HA, Polman A. Plasmonics for improved photovoltaic devices. Nat Mater 2010;9:205–13.
[19] Boriskina SV, Ghasemi H, Chen G. Plasmonic materials for energy: from physics to applications. Mater Today 2013;16:375–86.
[20] Lee HW, Papadakis G, Burgos SP, et al. Nanoscale conducting oxide PlasMOStor. Nano Lett 2014;14:6463–8.
[21] Liu N, Weiss T, Mesch M, et al. Planar metamaterial analogue of electromagnetically induced transparency for plasmonic sensing. Nano Lett 2010;10:1103–7.
[22] Wu C, Khanikaev AB, Adato R, et al. Fano-resonant asymmetric metamaterials for ultrasensitive spectroscopy and identification of molecular monolayers. Nat Mater 2012;11:69–75.
[23] Sönnichsen C, Franzl T, Wilk T, von Plessen G, Feldmann J. Drastic reduction of plasmon damping in gold nanorods. Phys Rev Lett 2002;88:077402.
[24] Endriz J, Spicer W. Surface-plasmon-one-electron decay and its observation in photoemission. Phys Rev Lett 1970;24:64–8.
[25] Fuchs R, Kliewer K. Surface plasmon in a semi-infinite free-electron gas. Phys Rev B 1971;3:2270–8.
[26] Inagaki T, Kagami K, Arakawa E. Photoacoustic observation of nonradiative decay of surface plasmons in silver. Phys Rev B 1981;24:3644–6.
[27] Clavero C. Plasmon-induced hot-electron generation at nanoparticle/metal-oxide interfaces for photovoltaic and photocatalytic devices. Nat Photonics 2014;8:95–103.
[28] White TP, Catchpole KR. Plasmon-enhanced internal photoemission for photovoltaics: theoretical efficiency limits. Appl Phys Lett 2012;101:073905.
[29] Leenheer AJ, Narang P, Lewis NS, Atwater HA. Solar energy conversion via hot electron internal photoemission in metallic nanostructures: efficiency estimates. J Appl Phys 2014;115:134301.
[30] Govorov AO, Zhang H, Gun'ko YK. Theory of photoinjection of hot plasmonic carriers from metal nanostructures into semiconductors and surface molecules. J Phys Chem C 2013;117:16616–31.
[31] Manjavacas A, Liu JG, Kulkarni V, Nordlander P. Plasmon-induced hot carriers in metallic nanoparticles. ACS Nano 2014;8:7630–8.
[32] Sundararaman R, Narang P, Jermyn AS, Goddard III WA, Atwater HA. Theoretical predictions for hot-carrier generation from surface plasmon decay. Nat Commun 2014;5:5788.
[33] Khurgin JB. How to deal with the loss in plasmonics and metamaterials. Nat Nanotechnol 2015;10:2–6.
[34] Brongersma ML, Halas NJ, Nordlander P. Plasmon-induced hot carrier science and technology. Nat Nanotechnol 2015;10:25–34.
[35] Baffou G, Quidant R. Thermo-plasmonics: using metallic nanostructures as nano-sources of heat. Laser Photon Rev 2013;7:171–87.
[36] Coppens ZJ, Li W, Walker DG, Valentine JG. Probing and controlling photothermal heat generation in plasmonic nanostructures. Nano Lett 2013;13:1023–8.
[37] Barnes WL, Dereux A, Ebbesen TW. Surface plasmon subwavelength optics. Nature 2003;424:824–30.
[38] Linic S, Christopher P, Ingram DB. Plasmonic-metal nanostructures for efficient conversion of solar to chemical energy. Nat Mater 2011;10:911–21.
[39] Mukherjee S, Libisch F, Large N, et al. Hot electrons do the impossible: plasmon-induced dissociation of $H_2$ on Au. Nano Lett 2013;13:240–7.
[40] Mubeen S, Lee J, Singh N, Krämer S, Stucky GD, Moskovits M. An autonomous photosynthetic device in which all charge carriers derive from surface plasmons. Nat Nanotechnol 2013;8:247–51.
[41] Appavoo K, Wang B, Brady NF, et al. Ultrafast phase transition via catastrophic phonon collapse driven by plasmonic hot-electron injection. Nano Lett 2014;14:1127–33.
[42] Kang Y, Najmaei S, Liu Z, et al. Plasmonic hot electron induced structural phase transition in a $MoS_2$ monolayer. Adv Mater 2014;26:6467–71.
[43] Naik GV, Dionne JA. Photon upconversion with hot carriers in plasmonic systems. Appl Phys Lett 2015;107:133902.
[44] Knight MW, Sobhani H, Nordlander P, Halas NJ. Photodetection with active optical antennas. Science 2011;332:702–4.
[45] Goykhman I, Desiatov B, Khurgin J, Shappir J, Levy U. Locally oxidized silicon surface-plasmon Schottky detector for telecom regime. Nano Lett 2011;11:2219–24.
[46] Sobhani A, Knight MW, Wang Y, et al. Narrowband photodetection in the near-infrared with a plasmon-induced hot electron device. Nat Commun 2013;4:1643.
[47] Wang F, Melosh NA. Power-independent wavelength determination by hot carrier collection in metal-insulator-metal devices. Nat Commun 2013;4:1711.
[48] Li W, Valentine J. Metamaterial perfect absorber based hot electron photodetection. Nano Lett 2014;14:3510–4.
[49] Li W, Coppens ZJ, Besteiro LV, Wang W, Govorov AO, Valentine J. Circularly polarized light detection with hot electrons in chiral plasmonic metamaterials. Nat Commun 2015;6:8379.
[50] Kim J-H, Yeo J-S. Enhanced detection of broadband incoherent light with nanoridge plasmonics. Nano Lett 2015;15:2291–7.
[51] Loo C, Lowery A, Halas N, West J, Drezek R. Immunotargeted nanoshells for integrated cancer imaging and therapy. Nano Lett 2005;5:709–11.
[52] Neumann O, Feronti C, Neumann AD, et al. Compact solar autoclave based on steam generation using broadband light-harvesting nanoparticles. Proc Natl Acad Sci USA 2013;110:11677–81.

[53] Fang Z, Zhen YR, Neumann O, et al. Evolution of light-induced vapor generation at a liquid-immersed metallic nanoparticle. Nano Lett 2013;13:1736–42.
[54] Narang P, Sundararaman R, Atwater HA. Plasmonic hot carrier dynamics in solid-state and chemical systems for energy conversion. Nanophotonics 2016;5:96–111.
[55] Fowler RH. The analysis of photoelectric sensitivity curves for clean metals at various temperatures. Phys Rev 1931;38:45–56.
[56] Spicer W. Photoemissive, photoconductive, and optical absorption studies of alkali-antimony compounds. Phys Rev 1958;112:114–22.
[57] Spicer WE. Negative affinity 3-5 photocathodes: their physics and technology. Appl Phys 1977;12:115–30.
[58] Lee H, Lee YK, Hwang E, Park JY. Enhanced surface plasmon effect of $Ag/TiO_2$ nanodiodes on internal photoemission. J Phys Chem C 2014;118:5650–6.
[59] Sze SM, Ng KK. Physics of semiconductor devices. 3rd ed. New Jersey: John Wiley, Sons, Inc., 2007, p. 682.
[60] Xue H, et al. Fabrication of $TiO_2$ Schottky barrier diodes by RF magnetron sputtering. In: 3rd IEEE International Conference on Nano/Micro Engineered and Molecular Systems, 2008, pp. 108–11.
[61] Huang J-J, Kuo C-W, Chang W-C, Hou T-H. Transition of stable rectification to resistive-switching in $Ti/TiO_2/Pt$ oxide diode. Appl Phys Lett 2010;96:262901.
[62] Carroll DL, Wagner M, Rühle M, Bonnell DA. Schottky-barrier formation at nanoscale metal-oxide interfaces. Phys Rev B 1997;55:9792–9.
[63] Wang X, Liow C, Qi D, et al. Programmable photo-electrochemical hydrogen evolution based on multi-segmented CdS-Au nanorod arrays. Adv Mater 2014;26:3506–12.
[64] Lieten RR, Afanas'ev VV, Thoan NH, Degroote S, Walukiewicz W, Borghs G. Mechanisms of Schottky barrier control on n-type germanium using $Ge_3N_4$ interlayers. J Electrochem Soc 2011;158:H358.
[65] Henkel C, Abermanna S, Bethge O, et al. Reduction of the PtGe/Ge electron Schottky-barrier height by rapid thermal diffusion of phosphorous dopants. J Electrochem Soc 2010;157:H815.
[66] Lee YK, Jung CH, Park J, Seo H, Somorjai GA, Park JY. Surface plasmon-driven hot electron flow probed with metal-semiconductor nanodiodes. Nano Lett 2011;11:4251–5.
[67] Bohren CF. How can a particle absorb more than the light incident on it? Am J Phys 1983;51:323.
[68] Zheng BY, Zhao H, Manjavacas A, McClain M, Nordlander P, Halas NJ. Distinguishing between plasmon-induced and photo-excited carriers in a device geometry. Nat Commun 2015;6:7797.
[69] Govorov AO, Zhang H. Kinetic density functional theory for plasmonic nanostructures: breaking of the plasmon peak in the quantum regime and generation of hot electrons. J Phys Chem C 2015;119:6181–94.
[70] Li X, Xiao D, Zhang, Z. Landau damping of quantum plasmons in metal nanostructures. N J Phys 2013;15:023011.
[71] Zhang H, Govorov AO. Optical generation of hot plasmonic carriers in metal nanocrystals: the effects of shape and field enhancement. J Phys Chem C 2014;118:7606–14.
[72] Gong T, Munday JN. Materials for hot carrier plasmonics. Opt Mater Express 2015;5:2501.
[73] Besteiro LV, Govorov AO. Amplified generation of hot electrons and quantum surface effects in nanoparticle dimers with plasmonic hot spots. J Phys Chem C 2016;120:19329–39.
[74] Kumarasinghe CS, Premaratne M, Gunapala SD, et al. Theoretical analysis of hot electron injection from metallic nanotubes into a semiconductor interface. Phys Chem Chem Phys 2016;18:18227–36.
[75] Kumarasinghe CS, Premaratne M, Bao Q, Agrawal GP. Theoretical analysis of hot electron dynamics in nanorods. Sci Rep 2015;5:12140.
[76] Bernardi M, Mustafa J, Neaton JB, Louie SG. Theory and computation of hot carriers generated by surface plasmon polaritons in noble metals. Nat Commun 2015;6:7044.
[77] Boriskina SV, Zhou J, Hsu W-C, Liao B, Chen G. Limiting efficiencies of solar energy conversion and photo-detection via internal emission of hot electrons and hot holes in gold. In: Proc. SPIE Infrared Remote Sensing and Instrumentation XXIII 960816, 2015.
[78] Chang YJ, Shih KH. Solar energy conversion via internal photoemission in aluminum, copper and silver: band structure effects and theoretical efficiency estimates. J Appl Phys 2016;119:183101.
[79] Brown AM, Sundararaman R, Narang P, Goddard III WA, Atwater HA. Non-radiative plasmon decay and hot carrier dynamics: effects of phonons, surfaces and geometry. ACS Nano 2016;10:957–66.
[80] Peters DW. An infrared detector utilizing internal photoemission. Proc IEEE 1967;55:704–5.
[81] Liu MY, Chou SY. Internal emission metal-semiconductor-metal photodetectors on Si and GaAs for 1.3 μm detection. Appl Phys Lett 1995;66:2673.
[82] Fukuda M, Aihara T, Yamaguchi K, Ling YY, Miyaji K, Tohyama M. Light detection enhanced by surface plasmon resonance in metal film. Appl Phys Lett 2010;96:153107.
[83] Faris S, Gustafson T, Wiesner J. Detection of optical and infrared radiation with DC-biased electron-tunneling metal-barrier-metal diodes. IEEE J Quant Electron 1973;9:737–45.
[84] Heiblum M, Whinnery J, Gustafson T. Characteristics of integrated MOM junctions at DC and at optical frequencies. IEEE J Quant Electron 1978;14:159–69.
[85] Goykhman I, Desiatov B, Khurgin J, Shappir J, Levy U. Waveguide based compact silicon Schottky photodetector with enhanced responsivity in the telecom spectral band. Opt Express 2012;20:28594–602.
[86] Knight MW, Wang Y, Urban AS, et al. Embedding plasmonic nanostructure diodes enhances hot electron emission. Nano Lett 2013;13:1687–92.
[87] Casalino M, Iodice M, Sirleto L, Rendina I, Coppola G. Asymmetric MSM sub-bandgap all-silicon photodetector with low dark current. Opt Express 2013;21:28072.
[88] Nazirzadeh MA, Atar FB, Turgut BB, Okyay AK. Random sized plasmonic nanoantennas on silicon for low-cost broad-band near-infrared photodetection. Sci Rep 2014;4:7103.
[89] Lin K-T, Chen H-L, Lai Y-S, Yu C-C. Silicon-based broadband antenna for high responsivity and polarization-insensitive photodetection at telecommunication wavelengths. Nat Commun 2014;5:3288.
[90] Desiatov B, Goykhman I, Mazurski N, Shappir J, Levy U. Plasmonic enhanced silicon pyramids for internal photoemission Schottky detectors in the near-infrared regime. Optica 2015;2:335.
[91] Ge J, Luo M, Zou W, et al. Plasmonic photodetectors based on asymmetric nanogap electrodes. Appl Phys Expr 2016;9:084101.

[92] Casalino M, Coppola G, De La Rue RM, Logan DF. State-of-the-art all-silicon sub-bandgap photodetectors at telecom and datacom wavelengths. Laser Photon Rev. doi:10.1002/lpor.201600065.
[93] Landy N, Sajuyigbe S, Mock J, Smith D, Padilla W. Perfect metamaterial absorber. Phys Rev Lett 2008;100:207402.
[94] Akselrod GM, Huang J, Hoang TB, et al. Large-area metasurface perfect absorbers from visible to near-infrared. Adv Mater 2015;27:8028–34.
[95] Giugni A, Torre B, Toma A, et al. Hot-electron nanoscopy using adiabatic compression of surface plasmons. Nat Nanotechnol 2013;8:845–52.
[96] Ueno K, Misawa H. Plasmon-enhanced photocurrent generation and water oxidation from visible to near-infrared wavelengths. NPG Asia Mater 2013;5:e61.
[97] Nishijima Y, Ueno K, Yokota Y, Murakoshi K, Misawa H. Plasmon-assisted photocurrent generation from visible to near-infrared wavelength using a Au-nanorods/$TiO_2$ electrode. J Phys Chem Lett 2010;1:2031–6.
[98] García de Arquer FP, Mihi A, Kufer D, Konstantatos G. Photoelectric energy conversion of plasmon-generated hot carriers in metal-insulator-semiconductor structures. ACS Nano 2013;7:3581–8.
[99] Shokri Kojori H, Yun JH, Paik Y, Kim J, Anderson WA, Kim SJ. Plasmon field effect transistor for plasmon to electric conversion and amplification. Nano Lett 2016;16:250–4.
[100] Sakhdari M, Hajizadegan M, Mohamed F, Chen PY. Efficient, broadband and wide-angle hot electron transduction using metal-semiconductor hyperbolic metamaterials. Nano Energy 2016;26:371–81.
[101] Wu BH, Liu WT, Chen TY, et al. Plasmon-enhanced photocatalytic hydrogen production on Au/$TiO_2$ nanocrystal arrays. Nano Energy 2016;27:412–9.
[102] Lee YK, Lee H, Park JY. Tandem-structured, hot electron based photovoltaic cell with double Schottky barriers. Sci Rep 2014;4:4580.
[103] Chalabi H, Schoen D, Brongersma ML. Hot-electron photodetection with a plasmonic nanostripe antenna. Nano Lett 2014;14:1374–80.
[104] Wang F, Melosh NA. Plasmonic energy collection through hot carrier extraction. Nano Lett 2011;11:5426–30.
[105] Wu K, Zhan Y, Zhang C, Wu S, Li X. Strong and highly asymmetrical optical absorption in conformal metal-semiconductor-metal grating system for plasmonic hot-electron photodetection application. Sci Rep 2015;5:14304.
[106] Wu K, Zhan Y, Wu S, Deng J, Li X. Surface-plasmon enhanced photodetection at communication band based on hot electrons. J Appl Phys 2015;118:063101.
[107] Zhan Y, Li X, Wu K, Wu S, Deng J. Coaxial Ag/ZnO/Ag nanowire for highly sensitive hot-electron photodetection. Appl Phys Lett 2015;106:081109.
[108] Gadalla MN, Abdel-Rahman M, Shamim A. Design, optimization and fabrication of a 28.3 THz nano-rectenna for infrared detection and rectification. Sci Rep 2014;4:4270.
[109] Grover S, Moddel G. Applicability of metal/insulator/metal (MIM) diodes to solar rectennas. IEEE J Photovoltaics 2011;1:78–83.
[110] Ward DR, Hüser F, Pauly F, Cuevas JC, Natelson D. Optical rectification and field enhancement in a plasmonic nanogap. Nat Nanotechnol 2010;5:732–6.
[111] Gong T, Munday JN. Angle-independent hot carrier generation and collection using transparent conducting oxides. Nano Lett 2015;15:147–52.
[112] Garcia de Arquer FP, Mihi A, Konstantatos G. Large-area plasmonic-crystal hot-electron based photodetectors. ACS Photonics 2015;2:950–7.
[113] Evans KM, Zolotavin P, Natelson D. Plasmon-assisted photoresponse in Ge-coated bowtie nanojunctions. ACS Photonics 2015;2:1192–8.
[114] Atar FB, Battal E, Aygun LE, Daglar B, Bayindir M, Okyay AK. Plasmonically enhanced hot electron based photovoltaic device. Opt Express 2013;21:7196.
[115] Lu Y, Dong W, Chen Z, et al. Gap-plasmon based broadband absorbers for enhanced hot-electron and photocurrent generation. Sci Rep 2016;6:30650.
[116] Chou JB, Li XH, Wang Y, et al. Surface plasmon assisted hot electron collection in wafer-scale metallic-semiconductor photonic crystals. Opt Express 2016;24:A1234–44.
[117] Harutyunyan H, Martinson AB, Rosenmann D, et al. Anomalous ultrafast dynamics of hot plasmonic electrons in nanostructures with hot spots. Nat Nanotechnol 2015;10:770–4.
[118] Akbari A, Berini P. Schottky contact surface-plasmon detector integrated with an asymmetric metal stripe waveguide. Appl Phys Lett 2009;95:021104.
[119] Scales C, Breukelaar I, Berini P. Surface-plasmon Schottky contact detector based on a symmetric metal stripe in silicon. Opt Lett 2010;35:529–31.
[120] Akbari A, Tait RN, Berini P. Surface plasmon waveguide Schottky detector. Opt Express 2010;18:8505–14.
[121] Casalino M, Sirleto L, Iodice M, et al. Cu/p-Si Schottky barrier-based near infrared photodetector integrated with a silicon-on-insulator waveguide. Appl Phys Lett 2010;96:241112.
[122] Casalino M, Iodice M, Sirleto L, Rao S, Rendina I, Coppola G. Low dark current silicon-on-insulator waveguide metal-semiconductor-metal-photodetector based on internal photoemissions at 1550 nm. J Appl Phys 2013;114:153103.
[123] Goykhman I, Sassi U, Desiatov B, et al. On-chip integrated, silicon-graphene plasmonic schottky photodetector with high responsivity and avalanche photogain. Nano Lett 2016;16:3005–13.
[124] Garín M, Fenollosa R, Alcubilla R, Shi L, Marsal LF, Meseguer F. All-silicon spherical-Mie-resonator photodiode with spectral response in the infrared region. Nat Commun 2014;5:3440.
[125] Liang TK, Tsang HK, Day IE, Drake J, Knights AP, Asghari M. Silicon waveguide two-photon absorption detector at 1.5 μm wavelength for autocorrelation measurements. Appl Phys Lett 2002;81:1323.
[126] Bradley JDB, Jessop PE, Knights AP. Silicon waveguide-integrated optical power monitor with enhanced sensitivity at 1550 nm. Appl Phys Lett 2005;86:241103.
[127] Ishii S, Inoue S, Ueda R, Otomo A. Optical detection in a waveguide geometry with a single metallic contact. ACS Photonics 2014;1:1089–92.
[128] Muehlbrandt S, Melikyan A, Harter H, et al. Silicon-plasmonic internal-photoemission detector for 40 Gbit/s data reception. Optica 2016;7:741.
[129] Huang YP, Wang LA. In-line silicon Schottky photodetectors on silicon cored fibers working in 1550 nm wavelength regimes. Appl Phys Lett 2015;106:191106.

[130] Bonaccorso F, Sun Z, Hasan T, Ferrari AC. Graphene photonics and optoelectronics. Nat Photonics 2010;4:611–22.
[131] Xia F, Wang H, Xiao D, Dubey M, Ramasubramaniam A. Two-dimensional material nanophotonics. Nat Photonics 2014;8:899–907.
[132] Dabidian N, Kholmanov I, Khanikaev AB, et al. Electrical switching of infrared light using graphene integration with plasmonic fano resonant metasurfaces. ACS Photonics 2015;2:216–27.
[133] Koppens FHL, Mueller T, Avouris P, Ferrari AC, Vitiello MS, Polini M. Photodetectors based on graphene, other two-dimensional materials and hybrid systems. Nat Nanotechnol 2014;9:780–93.
[134] Sun D, Aivazian G, Jones AM, et al. Ultrafast hot-carrier-dominated photocurrent in graphene. Nat Nanotechnol 2012;7:114–8.
[135] Echtermeyer TJ, Britnell L, Jasnos PK, et al. Strong plasmonic enhancement of photovoltage in graphene. Nat Commun 2011;2:458.
[136] Bao Y, Fang Z. Plasmon-enhanced photodetection in nanostructures. Nanotechnol Rev 2015;4:325–36.
[137] Fang Z, Wang Y, Schlather AE, et al. Active tunable absorption enhancement with graphene nanodisk arrays. Nano Lett 2014;14:299–304.
[138] Fang Z, Thongrattanasiri S, Schlather A, et al. Gated tunability and hybridization of localized plasmons in nanostructured graphene. ACS Nano 2013;7:2388–95.
[139] Fang Z, Liu Z, Wang Y, Ajayan PM, Nordlander P, Halas NJ. Graphene-antenna sandwich photodetector. Nano Lett 2012;12:3808–13.
[140] Fang Z, Wang Y, Liu Z, et al. Plasmon-induced doping of graphene. ACS Nano 2012;6:10222–8.
[141] Sobhani A, Lauchner A, Najmaei S, et al. Enhancing the photocurrent and photoluminescence of single crystal monolayer $MoS_2$ with resonant plasmonic nanoshells. Appl Phys Lett 2014;104:031112.
[142] Li Z, Ye R, Feng R, et al. Graphene quantum dots doping of $MoS_2$ monolayers. Adv Mater 2015;27:5235–40.
[143] Li Z, Xiao Y, Gong Y, et al. Active light control of the $MoS_2$ monolayer exciton binding energy. ACS Nano 2015;9:10158–64.
[144] Kang Y, Gong Y, Hu Z, et al. Plasmonic hot electron enhanced $MoS_2$ photocatalysis in hydrogen evolution. Nanoscale 2015;7:4482–8.
[145] Wang W, Klots A, Prasai D, et al. Hot electron-based near-infrared photodetection using bilayer $MoS_2$. Nano Lett 2015;11:7440–7.
[146] Gilbertson AM, Francescato Y, Roschuk T, et al. Plasmon-induced optical anisotropy in hybrid graphene-metal nanoparticle systems. Nano Lett 2015;15:3458–64.
[147] Lei S, Wen F, Ge L, et al. An atomically layered InSe avalanche photodetector. Nano Lett 2015;15:3048–55.
[148] Kern J, Andreas Trügler, Iris Niehues, et al. Nanoantenna-enhanced light-matter interaction in atomically thin $WS_2$. ACS Photonics 2015;2:1260–5.
[149] Fang Y, Verre R, Shao L, et al. Hot electron generation and cathodoluminescence nanoscopy of chiral split ring resonators. Nano Lett 2016;16:5183–90.
[150] Nusir A, Abbey GP, Hill AM, et al. Hot electrons in microscale thin-film schottky barriers for enhancing near-infrared detection. IEEE Photon Technol Lett 2016;28:2241–4.
[151] Lu Y-J, Kim J, Chen HY, et al. Plasmonic nanolaser using epitaxially grown silver film. Science 2012;337:450–3.
[152] High AA, Devlin RC, Dibos A, et al. Visible-frequency hyperbolic metasurface. Nature 2015;522:192–6.
[153] Ishii S, Shinde SL, Jevasuwan W, et al. Hot electron excitation from titanium nitride using visible light. ACS Photonics 2016;3:1552–7.
[154] Naldoni A, Guler U, Wang Z, et al. Enhancing hot carrier collection for solar water splitting with plasmonic titanium nitride. arXiv 2016;1607.06595.
[155] Ahmadivand A, Sinha R, Vabbina PK, et al. Hot electron generation by aluminum oligomers in plasmonic ultraviolet photodetectors. Opt Express 2016;12:13665–78.
[156] Wen L, Chen Q. Ultrathin continuous lossy metal film for broadband light absorption and hot electron collection. J Photon Energy 2016;6:042503.
[157] Wu K, Chen J, McBride JR, Lian T. Efficient hot-electron transfer by a plasmon-induced interfacial charge-transfer transition. Science 2015;349, 632–5.
[158] Zhang Y, Yam C, Schatz GC. Fundamental limitations to plasmonic hot-carrier solar cells. J Phys Chem Lett 2016;7:1852–8.
[159] Sze SM, Moll JL, Sugano T. Range-energy relation of hot electrons in gold. Solid State Electron 1964;7:509–23.
[160] Saavedra JRM, Asenjo-Harcia A, Garcia de Abajo FJ. Hot-electron dynamics and thermalization in small metallic nanoparticles. ACS Photonics 2016;Articel ASAP.
[161] Mejard R, Verdy A, Petit M, et al. Energy-resolved hot-carrier relaxation dynamics in monocrystalline plasmonic nanoantennas. ACS Photonics 2016;3:1482–8.
[162] Pelayo García de Arquer F, Mihi A, Konstantatos G. Molecular interfaces for plasmonic hot electron photovoltaics. Nanoscale 2015;7:2281–8.